# Control Strategies with Dynamic Threshold Adjustment for Supercapacitor Energy Storage System Considering the Train and Substation Characteristics in Urban Rail Transit

**Fei Lin \*, Xuyang Li, Yajie Zhao and Zhongping Yang**

School of Electrical Engineering, Beijing Jiaotong University, No.3 Shangyuancun, Beijing 100044, China; 14121438@bjtu.edu.cn (X.L.); 12121590@bjtu.edu.cn (Y.Z.); zhpyang@bjtu.edu.cn (Z.Y.)

**\*** Correspondence: flin@bjtu.edu.cn; Tel.: +86-10-51687064

**Abstract:** Recuperation of braking energy offers great potential for reducing energy consumption in urban rail transit systems. The present paper develops a new control strategy with variable threshold for wayside energy storage systems (ESSs), which uses the supercapacitor as the energy storage device. First, the paper analyzes the braking curve of the train and the *V-I* characteristics of the substation. Then, the current-voltage dual-loop control method is used for ESSs. Next, in order to achieve the best energy-saving effect, the paper discusses the selection principle of the charge and discharge threshold. This paper proposes a control strategy for wayside supercapacitors integrated with dynamic threshold adjustment control on the basis of avoiding the onboard braking chopper's operation. The proposed control strategy is very useful for obtaining good performance, while not wasting any energy in the braking resistor. Therefore, the control strategy has been verified through simulations, and experimental tests, have been implemented on the Batong Line of Beijing subway using the 200 kW wayside supercapacitor energy storage prototype. The experimental results show that the proposed control is capable of saving energy and considerably reducing energy consumption in the braking resistor during train braking.

## 1. Introduction

With the continuous economic development in China in recent years, urban rail transit has also undergone rapid development. From 2003 to 2013, the operating mileage of China urban rail transit increased from 290.4 km to 2326.0 km, the highest in the world [1]. In the urban rail transit system, braking energy of the train is commonly fed back to the catenary through regenerative braking. However, due to the 24-pulse diode rectifier unit used in the traction substation, surplus regenerating energy cannot provide feedback to the medium-voltage power grid. When a train is braking, if there are no adjacent traction trains or energy storage devices that can absorb the regenerative energy, then the pantograph voltage would exceed the normal range, thus leading to the onboard braking chopper operating, *i.e.*, the braking energy is wasted by the resistor [2,3]. Even worse, regeneration cancellation may occur. Therefore, in order to maximize the use of electric braking energy, while reducing mechanical braking and resistor braking of urban rail trains, currently two main options are energy storage and energy feedback [4]. At present, the main storage devices available are batteries, supercapacitors and flywheels.

Flywheels present relatively high overall efficiencies and elevated energy and power densities. However, they have a potential risk of explosive shattering in case of catastrophic failure and they have higher mechanical structure requirements [5–7].

The batteries present high energy density with discharge times ranging from tens of minutes to hours, which can provide power for the vehicle running to the safe place if the power supply is cut off because of trouble. Besides, the batteries can be used in the urban rail transit to absorb the braking energy and reduce the voltage fluctuation of the DC bus. Their cycle life is shorter and the power density is relatively low.

The supercapacitors have higher power density. They are suitable for supplying power peaks and absorbing the braking power peaks. In addition, they have longer cycle life. In this paper, a cycle is defined as the supercapacitor is charged to the maximum and discharged to the minimum value, which is considered one cycle. However, there are many definitions for cycle life, and it is related to the control strategy [8,9]. Another added value is that, unlike batteries, which require complex algorithms to estimate the state of charge (SOC), the determination of supercapacitor SOC is easily obtained by measuring their terminal voltage [10,11]. The urban rail transit operation has frequent starts and stops, and voltage peaks obviously fluctuate; supercapacitors match the operational characteristics of urban rail transit.

Depending on the placement of the supercapacitor energy storage system (ESS), the ESSs can be divided into the two types: onboard and off-board. The onboard type ESSs can absorb one train's braking energy and decrease the transmission loss during the process of energy flow. There are many applications with ESSs onboard in the trams [12,13]. While installed, ESSs will increase the weight of vehicles. Besides, the vehicles need more space to install the ESSs, so it might not be suitable for the metro trains to install onboard ESSs.

The off-board ESSs are able to absorb the braking energy from all the vehicles linked to the contact lines and feed the energy back into the contact lines for subsequent accelerations. Stationary ESSs are usually placed in the traction station or along the contact lines. Due to this, the ESSs can reduce the volume requirement. Therefore, off-board ESSs are usually applied in subway systems [14–16].

According to the system function, the station type and line type can be used to describe the ESSs. The station type supercapacitor ESS is typically placed in the traction substation, as shown in Figure 1, mainly for the recovery of regenerative braking energy. The line type is set in the middle of the line, primarily to reduce the voltage drop [17,18].
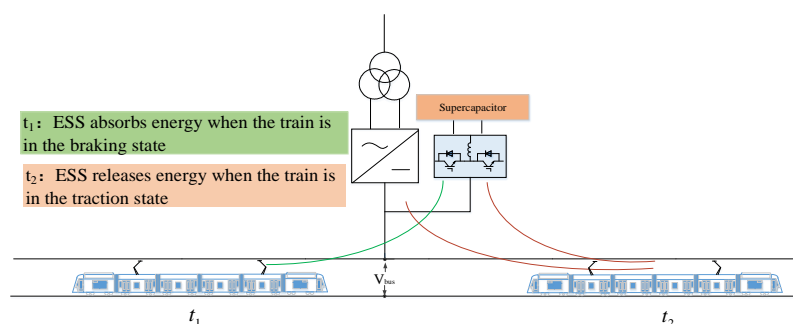


**Figure 1.** Operating principle of wayside supercapacitor energy storage system (ESS).

Station type supercapacitor ESSs usually use voltage and current bicyclic control method to achieve charging and discharging operations [19–21]. In [19], when the drive load switches from positive to negative (from motor mode to generator mode). The ultracapacitor begins to be charged until its voltage reaches the maximum reference $U_{C0max}$. The dc-bus voltage $V_{BUS}$ increases until it reaches the reference $V_{BUSmax}$. The magnitude of the current is adjusted by the cascaded controllers $G_{vBUSmax}$ and $G_{uC0}$ at this level, so as to maintain the dc-bus voltage constant. While the main is interrupted, the dc-bus voltage begins to decrease until it reaches the minimum reference $V_{BUSmin}$.

This allows deeper discharge of the ultracapacitor and regulation of the dc-bus voltage at the minimum $V_{BUSmin}$. However, the charging and discharging thresholds are all constants in [19–21], as they never change after setting.

However, these control methods do not analyze how to set the appropriate threshold, yet, charge and discharge threshold settings have extremely important impacts on the energy saving effect of the ESS [22–24]. This paper aims to acquire a control strategy of wayside ESSs, which is oriented to the optimization of the energy saving and reduction of the braking resistor's operation. The control is mainly based on the actual train braking characteristic, and takes the 24-pulse rectifier unit output characteristics into account. Due to the above characteristics analysis, a threshold setting study has been undertaken with the aim of better energy savings.

The organization of this work is as follows: The urban rail transit characteristics are analyzed in Section 2. Then, the wayside supercapacitor ESS compositions and its control strategy are introduced in Section 3. Next, Section 4 further analyzes the threshold selection strategy of the ESSs and a real-time adjustment of the threshold method is put forward. The simulation results are obtained in Section 5. Then, the experimental tests in the Beijing subway fully confirm the correctness of theoretical analysis, namely the threshold setting is closely related to the energy savings. Finally, Section 6 is the conclusion.

## 2. Analysis of Urban Rail Transit Characteristics

### 2.1. Braking Characteristics of the Trains

The braking curve of the induction traction motor in metro trains can be divided into three regions: constant torque, constant power and natural characteristics [25], shown as Equation (1) and Figure 2.

$$\begin{cases} F_t(v) = C_1 \\ F_t(v) \cdot V = C_2 \\ F_t(v) \cdot V^2 = C_3 \end{cases} \tag{1}$$

where $C_1$, $C_2$, and $C_3$ are constants, $F_t(v)$ is the traction effort and $V$ is the speed of the train.
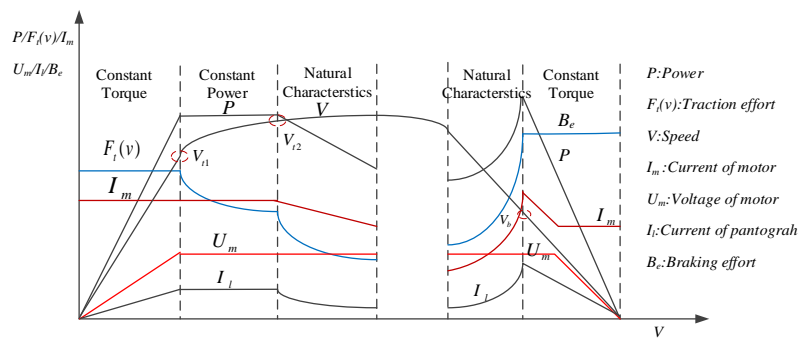


**Figure 2.** Traction/braking characteristics of metro train.

Taking trains from the Batong Line of Beijing subway in China as an example, the train brakes using air braking and electric braking, which includes regenerative braking and resistor braking. A brake control unit usually consists of M and T cars, and according to the train braking demand, electric braking acts first. Air braking force will compensate or substitute the electric braking when the electric braking force is insufficient or invalid.

When the electric braking operates, in order to prevent the DC voltage being beyond the permissible range, the controller controls the brake chopper throughout the voltage, across the filter capacitor of traction converters, to distribute the regenerative braking and resistor braking power. The working area of resistor braking is the shaded portion in Figure 3. Each inverter unit is equipped with a braking resistor, and the resistance is 1.203 Ω under room temperature. The regenerative

energy will give feedback to the grid first when the train is under electric braking, until the absorption capacity of the grid is insufficient. In addition to this, after the grid voltage is increased to 900 V, the resistor chopper will be activated. As the grid voltage gradually increases, the chopper working power gradually increases. The vehicle braking resistor operates at full power until reaching the maximum voltage of 1000 V.
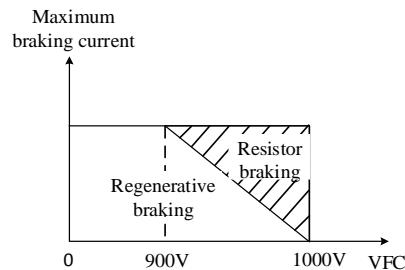


**Figure 3.** Mixed brake schematic of Batong train.

*2.2. Characteristics of the Equivalent 24-Pulse Rectifier*

The equivalent 24-pulse rectifier unit consists of two 12-pulse transformers and rectifiers, and the windings of the two rectifier transformers are moved to +7.5° and −7.5°, respectively, as shown in Figure 4.
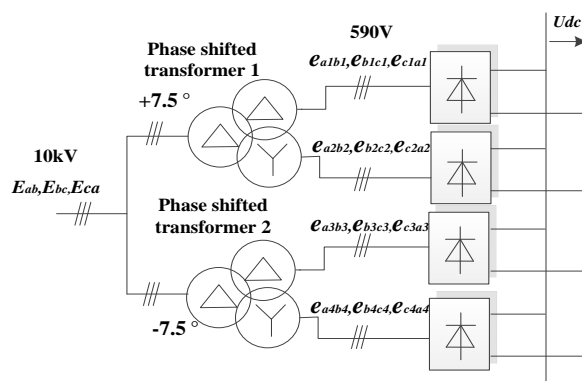


**Figure 4.** 24-pulse rectifier of the 750 V metro power supply system.

In multi-pulse rectifier technology, the output voltage $U_{dc0}$ of the rectifier unit is proportional to the grid-side no-load voltage [26].

$$\begin{cases} U_{d0} = \dfrac{P}{2\pi} \int_{\frac{\pi}{P}-\alpha}^{\frac{\pi}{P}+\alpha} \sqrt{2}U_2 \cos\theta \, d\theta = \dfrac{\sqrt{2}PU_2}{\pi} \sin\dfrac{\pi}{P}\cos\alpha \\[2mm] \qquad\qquad U_2 = NU_1 \\[2mm] \qquad\qquad U_1 = U_{1N}(1+\delta\%) \end{cases} \tag{2}$$

In Equation (2), $U_{d0}$ is the rectifier output no-load voltage, $P$ is the number of pulses, $U_2$ is the voltage of the valve side, $U_1$ is the line voltage of medium-voltage grid, $N$ is the turns ratio of transformer primary to secondary, $U_{1N}$ is the rating line voltage of medium voltage network and $\delta$ is the fluctuation ratio. The output voltage of the 24-pulse rectifier without load can be derived from Equation (3) as follows:

$$U_{dc0} \approx 1.41 NU_1 \tag{3}$$

As the load current increases, the output DC voltage of the equivalent 24-pulse rectifier unit reduces accordingly.

The external characteristic is mainly related to the impedance of the rectifier transformer, the topology of the rectifier circuit, the impedance of the AC power system, the operation status of the rectifier, and so on. According to engineering experience, the DC output voltage $U_{dc}$ of the 24-pulse rectifier unit can be calculated using the following equation [27]:

$$U_{dc} = U_o - \frac{k_r U_d}{100} \times \frac{U_n^2}{0.9 n S_T} \times I_{sub} \tag{4}$$

where $U_n$ represents the rating voltage of the DC side (kV), $U_d$ is the short-circuit voltage percentile of the transformer, $S_T$ is the capacity of the transformer (MVA), $n$ is the number of 24-pulse rectifier, $k_r$ is the coefficient resistance and 0.9 is matching coefficient between the transformer and rectifier.

Based on the output voltage and current data measured at the Beijing subway traction substation, the output characteristics can be plotted as shown in Figure 5.
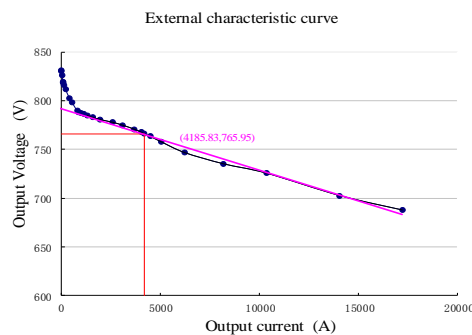


**Figure 5.** The output character of the 24-pulse rectifier.

When the output current is approximately 4185.8 A, the rated output voltage of traction substations is 765.9 V, at which time the load rate of traction substation is 100%. The output voltage of traction substation decreases as the output current increases, and the slope of the characteristic curve changes in pace with the output current increase.

## 3. Wayside Supercapacitor Energy Storage System and Control Strategy

### 3.1. System Components

The station type supercapacitor ESS consists of a bi-directional DC/DC converter and supercapacitor, as shown in Figure 6. The bi-directional DC/DC converter is the key component of the whole system, undertaking the tasks of system voltage level shift and energy management.
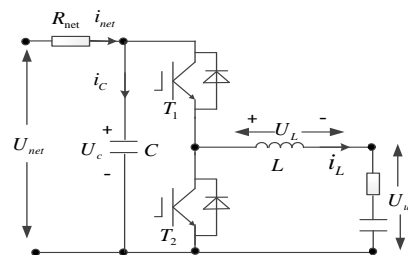


**Figure 6.** Supercapacitor storage system based on half-bridge topology.

Depending on different conditions of the traction substation, the supercapacitor ESS will operate when in charging or discharging status, the bidirectional DC/DC converter through control $T_1$ and $T_2$

switching to realize supercapacitor's charging or discharging, thus achieving the different directions of chopping inductor current $i_L$. Operating in either the charging or discharging status, the supercapacitor ESS can be represented using the unified model shown in Figure 7, where $R_{on}$ is the on-state resistance of the IGBT, $R_L$ is the equivalent resistance of the chopping inductor, $R_{net}$ is the equivalent resistance of the input side, and $R_{uc}$ is the ESR of the supercapacitor.
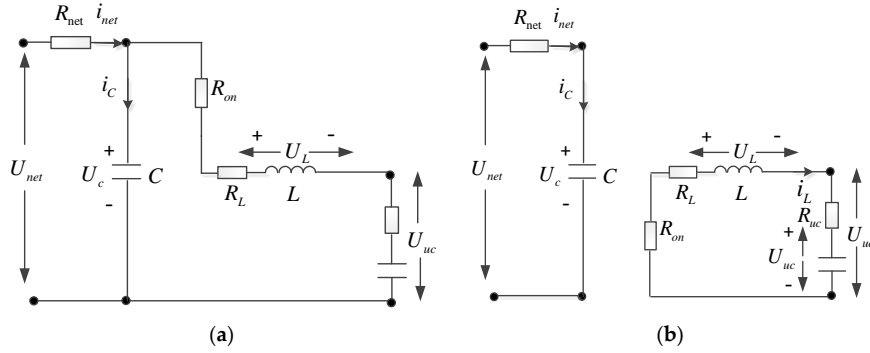


**Figure 7.** Equivalent model of supercapacitor storage system in switching period. (**a**) $0 < t < DT_s$; (**b**) $DT_s < t < T_s$.

### 3.2. System Control Strategy

The control module of the ESS can be divided into four parts, the overall control block diagram of which is shown in Figure 8.
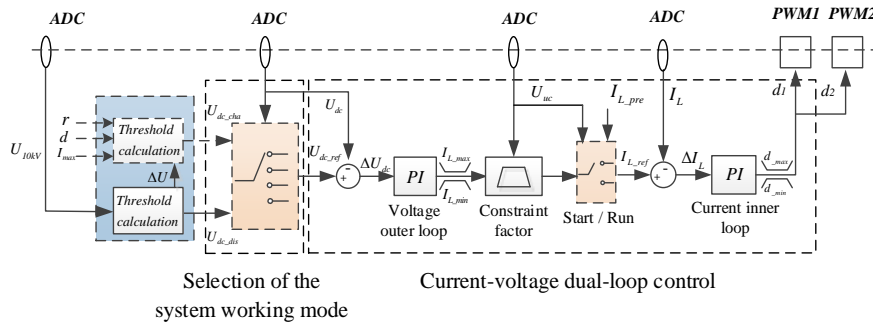


**Figure 8.** Control block diagram of wayside supercapacitor storage system.

### 3.2.1. Current-Voltage Dual-Loop Control

As shown in Figure 8, the system uses the cascade control strategy to control the DC bus voltage loop and supercapacitor current loop, and the controller uses the traditional PI control. During the controller design, the small signal analysis model of the supercapacitor ESS can be modeled through the state-space averaging method [28]. Each part of the system transfer function is shown as follows:

$$G_{id}(s) = \frac{\overset{\wedge}{i_L}}{\overset{\wedge}{d}} = \frac{(CRR_pU_{net} + CDR^2U_{uc})s + (R_p - D^2R)U_{net}}{CLR(D^2 + R_p)s^2 + [CD^2R^2R_p + (LD^2 + CR_p^2 + LR_p)]s + (D^4R^2 + 2DR_m + R_p^2)} \quad (5)$$

$$G_{ud}(s) = \frac{\overset{\wedge}{u_c}}{\overset{\wedge}{d}} = \frac{LR_L(U_{uc} - DU_{net})s + [(D^2R_L^2 + R_n + R_z)U_{uc} - 2D(R_n + R_z)U_{net}]}{CLR(D^2 + R_p)s^2 + [CD^2R^2R_p + (LD^2 + CR_p^2 + LR_p)]s + (D^4R^2 + 2DR_m + R_p^2)} \quad (6)$$

where $G_{id}$ is the transfer function of the supercapacitor current to the duty cycle, and $G_{ud}$ denotes the transfer function of the bus voltage to the duty cycle. $R = R_{net}$, $R_p = R_{on} + R_L$, $R_m = R_{on} \cdot R_{net}$, $R_n = R_{net} \cdot R_L$, $R_z = R_{on} \cdot R_L$.

### 3.2.2. Selection of the System Working Mode

In view of the different operating states of the train and achieving the multi-modal switchover, the working area of the supercapacitor ESS must be selected to reasonably realize recycling braking energy. Therefore, based on the voltage state of the traction power supply, the workspace is divided as shown in Figure 9.
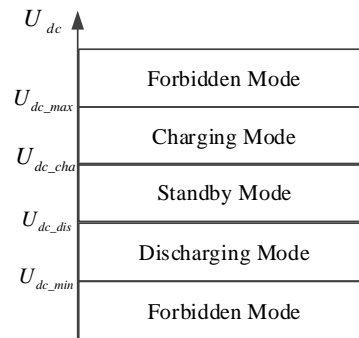


**Figure 9.** Principle of mode-transition.

On the one hand, the discharge and charge threshold are the switching symbols of different modes, while on the other hand they are also the target regulation values of outer voltage loop of the traction grid. Therefore, the design and selection of the threshold determine whether the ESS can work, and even whether it can work in the best possible state.

## 4. Threshold Selection of Wayside Supercapacitor Energy Storage System

### 4.1. Analysis of the Discharge Threshold's Impact and Setting Methods

In the discharge mode, in order to analyze the whole system, including traction substations, ESSs and train loading system, a model is constructed (Figure 10).

The relationship among the parameters in Figure 10 can be obtained as follows:

$$i_{\text{LOAD}} = i_{\text{SUB}} + i_{\text{ESS}} \tag{7}$$

$$V_{\text{REC}} = V_{\text{REC0}} - i_{\text{SUB}} \cdot R_{\text{REC}} \tag{8}$$

Parameter $i_{\text{LOAD}}$ is the load current of the train, $i_{\text{SUB}}$ is the output current of the traction substation, $i_{\text{ESS}}$ is the output current of supercapacitor ESS in the high voltage side, $V_{\text{REC0}}$ is the output no load voltage of the rectifier unit, and $V_{\text{REC}}$ is the output voltage of rectifier unit.
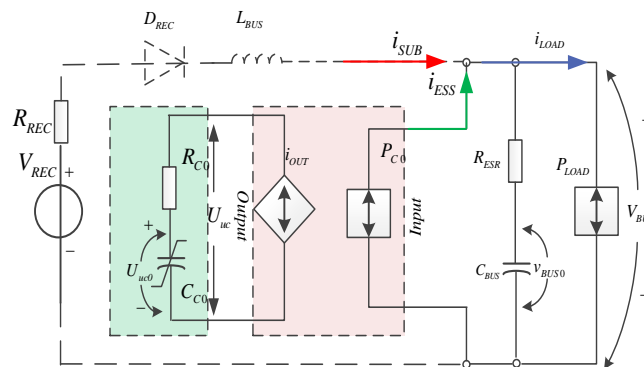


**Figure 10.** System structure during the discharging mode.

Under the condition that the power of the storage system matches with the braking power of the train, the relationship between the discharge threshold of the ESS and the output voltage of the traction substation can be shown as Equation (9):

$$V_{\text{REC}} = V_{\text{REC0}} - i_{\text{SUB}} \cdot R_{\text{REC}} = U_{\text{dc\_dis}} \tag{9}$$

The energy storage device output coefficients $\alpha$ is defined as Equation (10), which is used to signify the output situation of the energy storage device and the traction substation:

$$\alpha = \frac{i_{\text{ESS}}}{i_{\text{LOAD}}} \tag{10}$$

Based on Equations (7)–(10), under different values of $i_{\text{LOAD}}$, how the setting of discharge threshold affects the energy storage device output coefficients is shown in Figure 11.
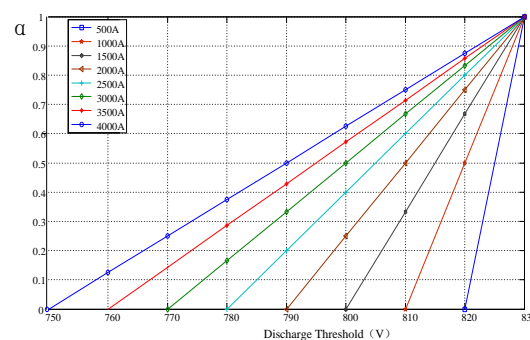


**Figure 11.** Influence of $U_{\text{dc\_dis}}$ to $\alpha$.

From Figure 11, we take the current curve as an example when the load current of train is 2000 A. In the case of the discharge threshold being 830 V (output voltage of the rectifier when there is no load), the output coefficient of the storage system is 1. Nevertheless, the output coefficient decreases linearly as the discharge threshold lessens. When set to 805 V, the output factor of energy storage device is 0.5, *i.e.*, the energy storage device and traction substation bear equal load currents. The worst situation occurs when the discharge threshold is set at 780 V or lower, and the output coefficient of the storage device is 0, indicating that the load current is entirely borne by the traction substation and the storage device is no longer bearing the load current, namely the storage energy devices cannot effectively release the energy stored.

In order to achieve recycling the regenerative braking energy, the energy storage device shall ensure an adequate energy margin, thus considering the requirement that the energy storage device releases energy effectively, and thus the control strategy discharge threshold should preset as Equation (11):

$$U_{\text{dc\_dis}} = V_{\text{REC0}} \tag{11}$$

*4.2. Analysis of the Charge Threshold and Its Impacts*

The charge threshold is not only the flag that the storage system runs into charging mode, but also the value of the voltage regulator of the outer loop. In the analysis of the train braking characteristics in Section 2.1, it is shown that when the DC bus voltage rises above 900 V, the braking chopper of the train will be put into operation to curb the bus voltage rising. The operation of the braking chopper means that the regenerative braking energy is almost entirely consumed in the braking resistor, which is unfavorable for saving energy. Therefore, the value of the charge threshold must be reasonable in order to make the voltage at the pantograph be no more than 900 V throughout, therefore allowing the braking resistor's operation to be avoided. This also means that the ESS maximizes the absorption of regenerative braking energy.

The metro power supply system can be divided into traction substation and step-down substation, and a supercapacitor ESS is typically installed in the traction substation. Traction substation and step-down substation are usually set on different metro stops, and the distance between the train braking point and the location of the supercapacitor can be divided into two conditions, as shown in Figure 12. The first is that the braking point is near the metro stop that has a traction substation, which also means that supercapacitor energy storage is performed, while the second is that the braking point is near the metro stop which has a step-down substation, meaning that it has a greater distance with energy storage device than the first circumstance.
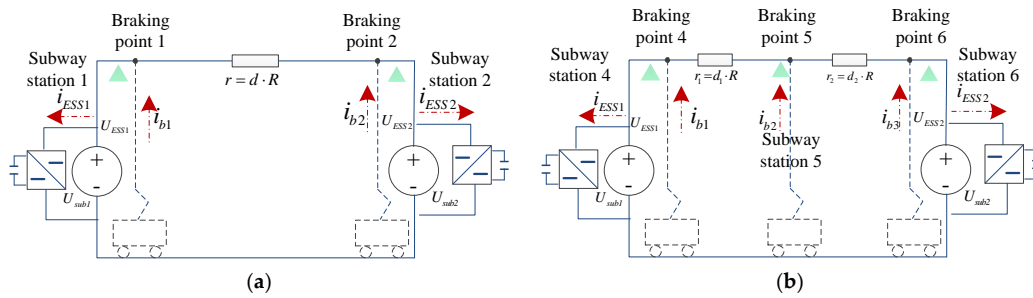


**Figure 12.** Metro power supply system with supercapacitor storage system: (**a**) Two subway stations with two braking points; (**b**) Three subway stations with three braking points.

In the first circumstance there are no subway stations contained in the middle of two subway stations, with train brakes on the adjacent sides of both stops, as shown in Figure 12a. Another case is that the train has at least three braking points, in which two cases are adjacent to the ESS and one situation is at a greater range, as shown in Figure 12b.

Figure 12a illustrates that the train braking point is in the vicinity of the ESS, thus the voltage drop caused by the line impedance is negligible. Unlike Figure 12a, in Figure 12b the train braking point is not only close to the supercapacitor system, it is also in the middle of the subway stations. The moment at which the voltage drop caused by the line impedance should be considered is shown in Figure 13. If the power and capacity of the ESS are sufficient to absorb electric braking energy, then the bus voltage of ESS side can be stabilized in charge threshold $U_{\text{dc\_cha}}$, and also satisfies the following equation:

$$U_{\text{dc\_dis}} = V_{\text{bus}} - r \cdot i_{\text{LOAD}} = V_{\text{bus}} - d \cdot R \cdot i_{\text{LOAD}} \tag{12}$$

where $V_{\text{bus}}$ is the voltage of train pantograph, $d$ is the distance between the braking point and the location of ESS, $R$ is the line impedance and $i_{\text{LOAD}}$ is the supercapacitor current regenerated by train braking.
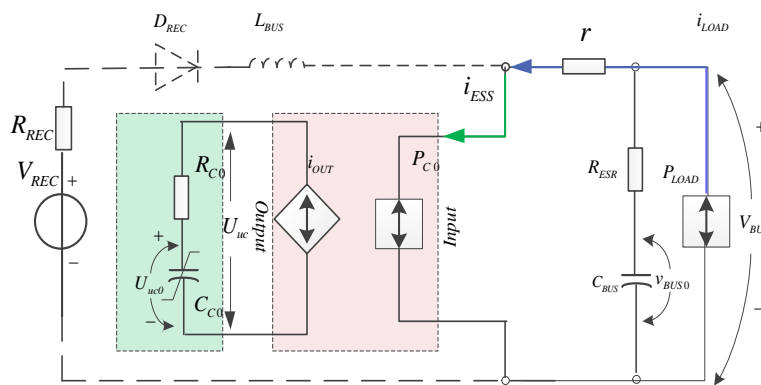


**Figure 13.** System structure during charging mode.

Defining the train braking energy conversion factor is β, which is used to characterize the electric train braking power conversion efficiency (Equation (13)):

$$\beta = \frac{i_{\text{LOAD}}}{i_{\text{REG}}} \tag{13}$$

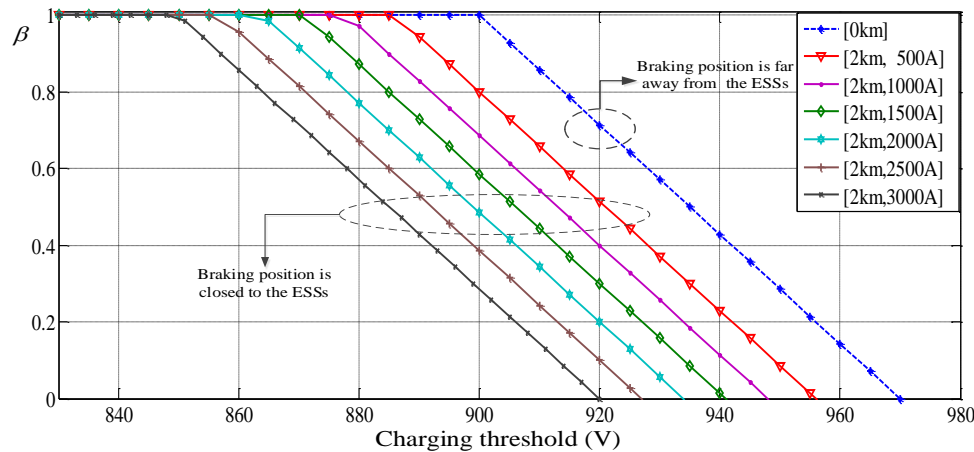The charge threshold's impact on the conversion factor is shown in Figure 14.



**Figure 14.** Influence of $U_{\text{dc\_cha}}$ to the β.

The following conclusions can be obtained through Figure 14.

(a)　If the train braking points are in the vicinity of the traction substation, which means being close to the supercapacitor storage system as well, then the line impedance is negligible. The charging threshold is between 830 V and 900 V, due to the fact that charging threshold is smaller than the threshold of 900 V, which is the brake chopper's start symbol. Based on this, the braking resistor does not operate, the electric braking energy is completely absorbed by the supercapacitor system, and the conversion factor of the electric braking power is constantly 1. When the charging threshold is set between 900 V and 970 V, β gradually decreases as the charge threshold increases, *i.e.*, the power of the braking resistor is growing, while the regenerative energy absorbed by the ESS becomes lower and lower. When the charging threshold is set at 970 V, β is 0, indicating that all of the regenerative energy of the train is consumed by resistor braking and mechanical braking.

(b)　In the case that the braking position and energy storage device has a far distance, which is assumed as 2 km, the line impedance of steel and aluminum contact rail unit is 0.0069 Ω/km. Taking 2000 A as the feedback current of the train as an example, the charge threshold value is set between 830 V and 860 V, the conversion factor of electric braking power is constantly 1. When the charging threshold is set between 860 V and 930 V, β gradually decreases as the charging threshold increases. The worst situation is when set at 930 V, and β is 0, indicating that all of the braking energy is consumed by the braking resistor and mechanical braking.

On the premise of ensuring that the power of energy storage device matches the braking power of the train, the regenerative braking energy of the train acquire get the feedback to the greatest extent, thus avoiding energy waste. The train braking point is not only close to the supercapacitor system, it is also in the middle of the subway stations. Taking the Figure 12b for example, there are three braking points. The distance between the two traction substations is defined as *d*. The distance between the braking position and ESS is from 0 to *d*. If the distance is chosen as *d*, when the vehicles brake near the ESSs, the charging threshold is too low. Considering the better effect of energy recovery in different braking points, the equivalent distance between the braking position and ESS can be chosen as *d*/2. No matter the vehicle brakes near or keep away the ESSs, the charging threshold is an eclectic selection.

$I_{max}$ is the maximum feedback current in the process of braking, which is calculated through traction calculation. Though the current $I$ is chosen at the maximum situation, the charging threshold keeps a relatively small value to ensure the ESSs can recycle the regenerative braking energy every time.

Therefore, considering the sufficient margin, the charge threshold value should be set as follows:

$$U_{dc\_cha} = U_{dc\_lim} - d_{equ} \cdot R \cdot I_{max} \tag{14}$$

$U_{dc\_lim}$ should be set as the start voltage threshold of the train braking chopper, and $d_{equ}$ is the equivalent distance between the braking position and ESS, which is chosen as $d/2$. $R$ is the impedance of contact rail, which is a constant determined by the contact rail material.

### 4.3. Dynamic Threshold Adjustment Strategy

The charging and discharging threshold effects and settings are discussed in Sections 4.1 and 4.2 respectively, and the above conclusions are analyzed under the ideal substation output voltage of 830 V without loads. Considering the fact that the traction substation takes non-ideal output characteristics into account, the control strategy of the wayside supercapacitor ESS is proposed based on dynamic threshold adjustment, shown in Figure 15, and it is the threshold calculation part of Figure 8.

To identify the output voltage of traction substation when there is no load, using the transformer grid side (10 kV) voltage as a reference variable, real-time load voltage value $V_{REC0}$ can be calculated by Equation (15), then discharge threshold $U_{dc\_dis}$ can also be obtained:

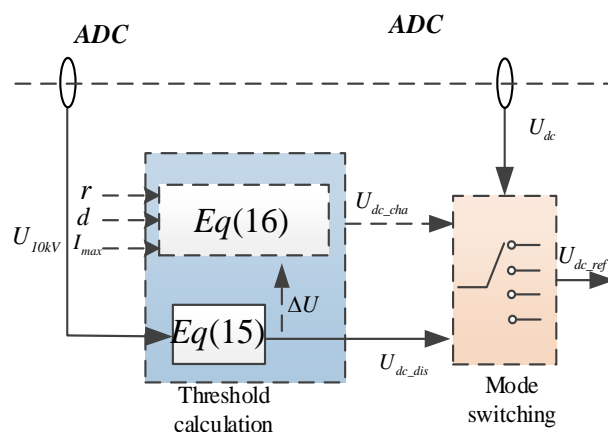$$U_{dc\_dis} = V_{REC0} = m \cdot n \cdot U_{10kV} \tag{15}$$



**Figure 15.** Control strategy based on dynamic threshold.

In Equation (15), $m$ is the coefficient between the 24-pulse rectifier transformer valve side to the DC output voltage of the rectifier, $n$ is the turns ratio coefficient of the primary side of the transformer to the valve side, and $U_{10kV}$ is the line voltage RMS of the transformer primary side. In the case of output voltage of the traction substation has fluctuations, in order to ensure the reliability of the modal switch in preventing accidental charging, the settings of the charging threshold in Equation (14) should be improved, shown as follows:

$$U_{dc\_cha} = \begin{cases} U_{dc\_lim} - d_{equ} \cdot R \cdot I_{max}; & (U_{dc\_lim} - d_{equ} \cdot R \cdot I_{max} \geqslant V_{REC0} + U_{\Delta}) \\ V_{REC0} + U_{\Delta} = m \cdot n \cdot U_{10kV} + U_{\Delta}; & (U_{dc\_lim} - d_{equ} \cdot R \cdot I_{max} < V_{REC0} + U_{\Delta}) \end{cases} \tag{16}$$

Most of the time, the charging threshold is determined by the equation $U_{dc\_cha} = U_{dc\_lim} - d_{equ}RI_{max}$; only when the calculated charging threshold is lower than the $V_{REC0} + U_{\Delta}$, the charging threshold should be set as $V_{REC0} + U_{\Delta}$ to avoid the ESSs charging falsely.

## 5. Simulation and Experimental Results

### 5.1. Simulation Platform and Parameters

Using Matlab/Simulink, we built a model including a 24-pulse rectifier unit, trains and a supercapacitor ESS, which is shown as Figure 16.
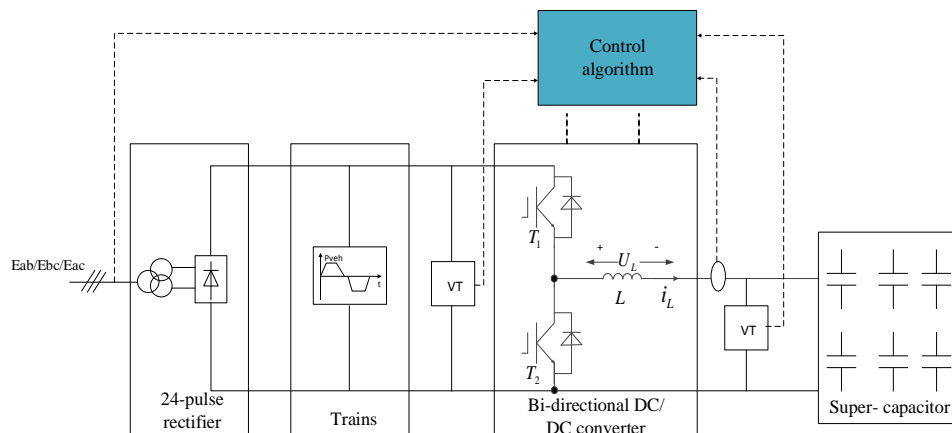


**Figure 16.** Simulation platform in Matlab/Simulink.

The simulation parameters are shown in Table 1.

**Table 1.** Simulation parameters.

|                 |                   |            |
| --------------- | ----------------- | ---------- |
| **Substation**  | $U_{1N}$          | 10 kV      |
|                 | $U_{1N}:U_{2N}$   | 10,000:590 |
| **Storage system** | $L$            | 0.83 mH    |
|                 | $L_d$             | 1.5 mH     |
|                 | $C_{sc}$          | 31.5 F     |
|                 | $C_d$             | 5000 uF    |
|                 | $U_{dc\_cha}$     | 900 V      |

### 5.2. Simulation Results and Analysis

The line voltages of the transformer primary in the simulation were, respectively, given as 10, 9.3 and 10.7 kV. The simulation results are shown in Figure 17; when the medium-voltage grid voltage is 10 kV, the discharge threshold is adjusted to 830 V automatically. Another case, when grid voltage is 9.3 kV, the discharge threshold is adjusted to 770 V. While the grid voltage is 10.7 kV, the discharge threshold value is adjusted to 880 V. The supercapacitor ESS in the process of the above changes achieves the release of energy in a reliable way, and also verifies the feasibility of the policy based on dynamic threshold adjustment.
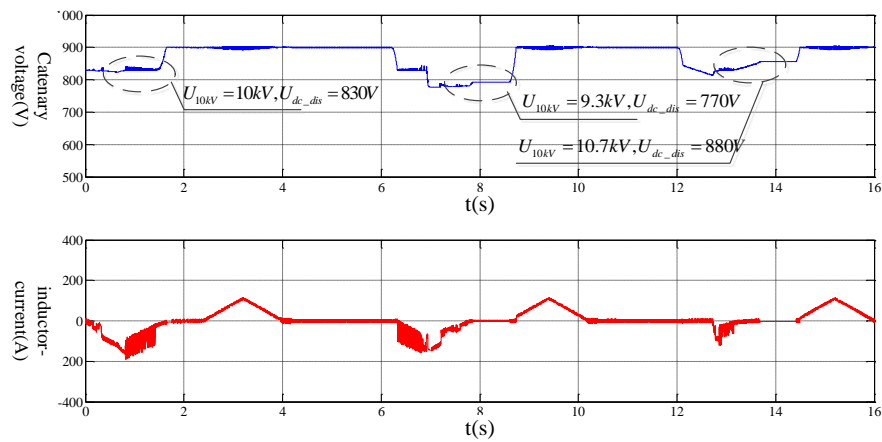
**Figure 17.** Simulation result of dynamic voltage threshold.

*5.3. Experimental Conditions*

In order to verify the feasibility of the control algorithm, a 200 kW wayside supercapacitor ESS was developed. The system was installed in the Tongzhou Beiyuan substation of the Batong Line of the Beijing subway system, and tests were conducted during the day when the Batong Line is under normal operation. Based on these experiments, the control method's correctness has been verified. The ESS is shown in Figure 18.
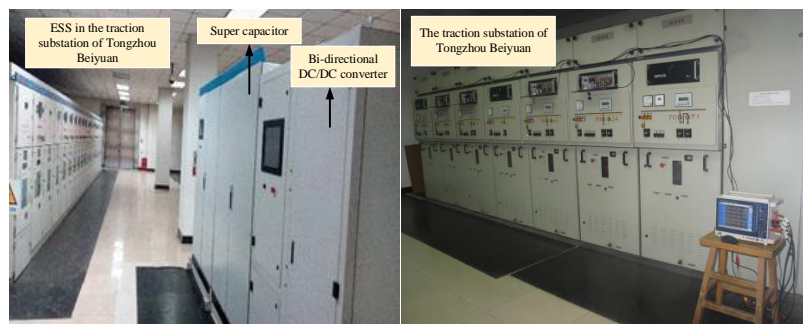


**Figure 18.** Supercapacitor ESS installed in substation.

The system design parameters are shown in Table 2, and the bidirectional DC/DC converter rated power is 200 kW, wherein the high side input voltage is 500–1000 V, rated working voltage is 750 V and the peak voltage of 1000 V. In addition, the low side output current is 0–400 A. Peaking power of supercapacitor is 200 kW, operating voltage range is from 0 V to 500 V and the operating current is 0–400 A. The maximum storage energy of supercapacitor is 0.944 kWh in total.

**Table 2.** Parameters of 200 kW wayside supercapacitor storage system.

| Parameters | | Value |
|---|---|---|
| Bi-directional DC/DC converter | Input voltage (V) | 500–1000 |
| | Input current (A) | 0–267 |
| | Output voltage (V) | 0–500 |
| | Output current (A) | 0–400 |
| Ultra capacitor | Working voltage (V) | 0–500 |
| | Working current(A) | 0–400 |
| | Maximum storage energy (kWh) | 0.944 |

The main wiring schematic of the Tongzhou Beiyuan traction substation in the Beijing Subway system is shown in Figure 19.
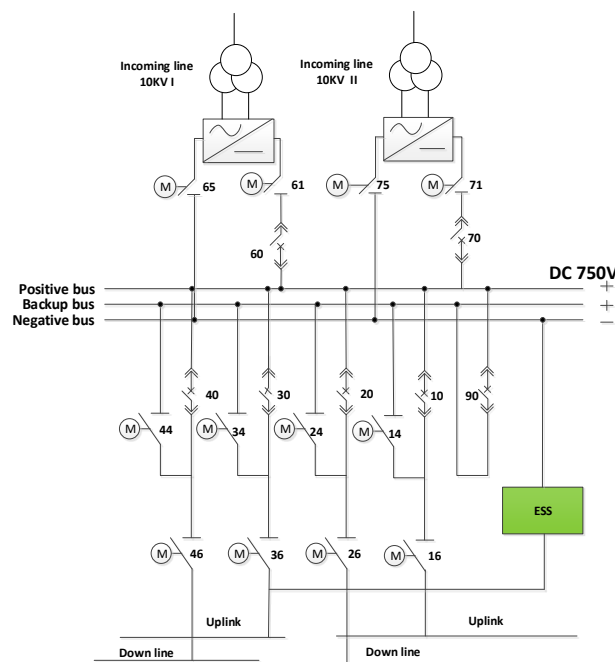


**Figure 19.** Primary connection of traction substation with supercapacitor storage system.

*5.4. Experimental Results and Analysis*

When the train is on the state of traction, the DC voltage drops, while along with the storage system's work, the DC voltage dropping degree can be suppressed. On the contrary, the DC voltage boosts when the train brakes. The supercapacitor storage system recycles the regenerative braking energy so as to suppress the DC voltage's increase. These are shown in Figure 20.
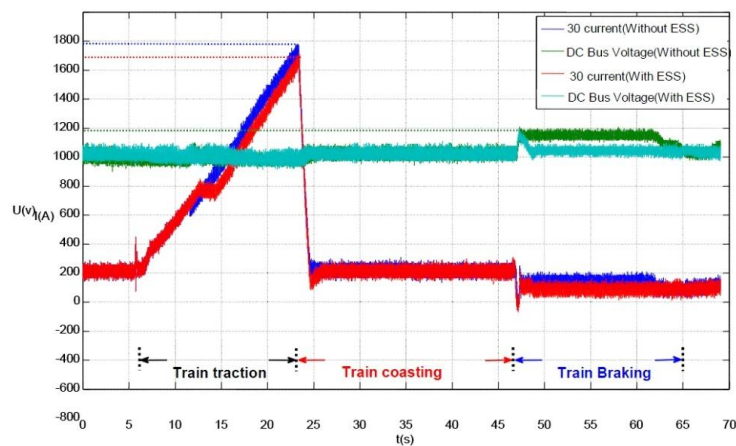


**Figure 20.** One Traction and braking cycle with and without ESS.

Next, tests are performed under circulation conditions, as shown in Figure 21. Through the above trials, the supercapacitor system can charge and discharge normally. In addition, it can also stabilize the DC voltage and save braking energy, which can be analyzed through the experiment waveform as follows.
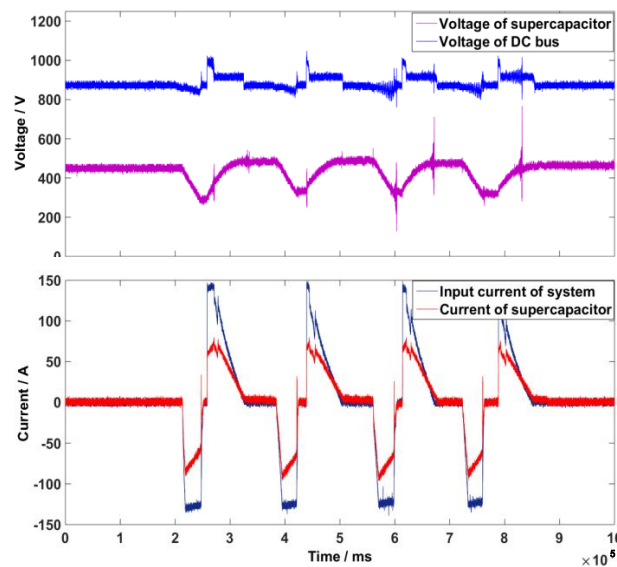
**Figure 21.** Waveforms in multiple cycles.

In Section 4.1, the influence of the discharge threshold is analyzed, and the analysis and conclusions are verified by experiments during night tests. In the night tests, the train runs four successive cycles (traction-coasting-braking), and the voltage and current of the supercapacitor energy storage prototype has been recorded by oscilloscope. During the experiment, the DC voltage without load is 830 V. In the process of the tests, the $U_{dc\_dis}$ was given as 805, 810 and 815 V, and the voltage of the supercapacitor is shown in Figure 22.
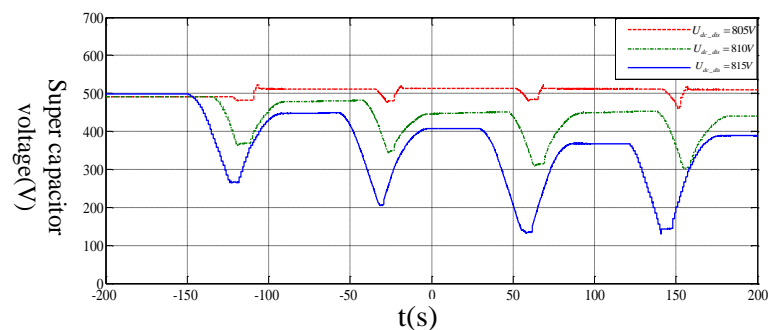


**Figure 22.** Influence of $U_{dc\_dis}$.

$E_{train}$ is on the behalf of the energy consumed by train at the traction stage, and $E_{uc}$ is the supercapacitor ESS's output energy. When discharge threshold $U_{dc\_dis}$ is 805, 810 and 815 V, the respective output coefficients are 2.6%, 13% and 25%. When the discharge threshold is closer to output voltage $V_{REC0}$ without load, the output coefficient of the supercapacitor ESS increases. When its power and traction power train match, the output coefficient can be up to 1, which is consistent with the theoretical analysis in Section 4.1.

The following tests are conducted during the day when there are many trains running with passengers. The charging threshold is constantly set to 890 V during the first test, and due to the presence of the line impedance, the threshold is set too high, thus the ESS basically does not absorb regenerative braking energy, as shown in Figure 23a. When the train is pulled, the bus voltage drops, the energy storage device discharges, the voltage of the supercapacitor changes from 500 V to 200 V. Because of unreasonable charging threshold settings, at the stage of train braking, the DC bus voltage rises, but no more than the charge threshold. Thus in the whole test cycle, energy storage device does

not absorb the regenerative braking energy basically. At this time, the regeneration braking energy can only be consumed by the braking resistor, which results in energy waste. The energy saving effect greatly reduces because the inappropriate threshold setting.

Then the dynamic threshold adjustment strategy was used, as shown in Figure 23b. The ESSs charging times are more in number, and absorbing more regeneration braking energy, which means that the energy saving effect of ESS is improving. During the test cycles, due to the appropriate threshold setting and the discharging threshold changes with the DC power supply system, the ESS shows good energy saving effect. At every test cycle, the supercapacitor can be charged to the maximum voltage 500 V when the train is braking and discharged to the minimum voltage 200 V when the train is in the state of traction, which means the ESS has fully absorbed the regenerative braking energy and released the energy to the traction power supply when the DC bus voltage drops.
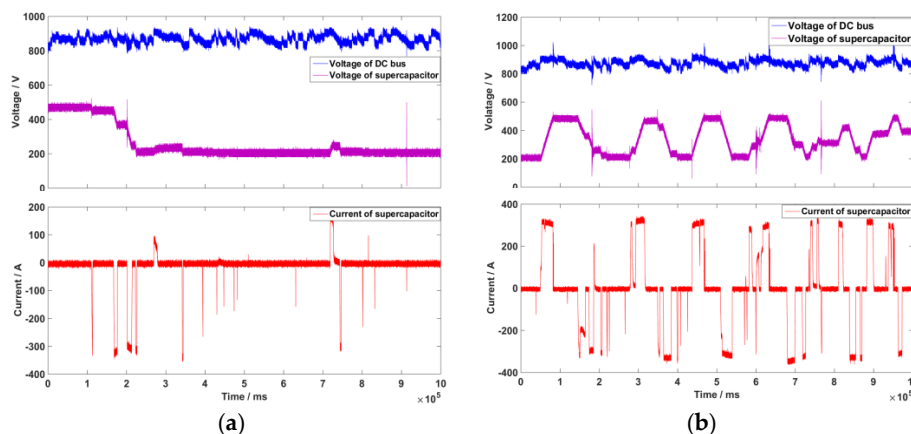


**Figure 23.** Threshold impacts on energy savings: (**a**) Charging threshold is 890V; (**b**) Dynamic threshold adjustment strategy.

## 6. Conclusions

In this study, based on the analysis of braking characteristics of urban rail transit train and 24-pulse traction substation characteristics, a control strategy is proposed to apply into the wayside supercapacitor ESS. On the one hand, the energy-saving and voltage stabilization effects of the supercapacitor applied to urban rail transit are verified through simulation and prototype test in Beijing subway, while on the other hand, the feasibility of the dynamic threshold adjustment control strategy is verified. In this paper, the research shows that the threshold of charge and discharge must be adjusted dynamically, and the performance is satisfactory.

**Author Contributions:** Fei Lin, Xuyang Li and Yajie Zhao contributed significantly to the analysis and manuscript preparation. Zhongping Yang contributed to the conception of the study.

**Conflicts of Interest:** The authors declare no conflict of interest.

## References

1. Qin, F.; Zhang, X.; Zhou, Q. Evaluating the impact of organizational patterns on the efficiency of urban rail transit systems in China. *J. Transp. Geogr.* **2014**, *40*, 89–99. [CrossRef]
2. Ogasa, M. Energy saving and environmental measures in railway technologies: Example with hybrid electric railway vehicles. *IEEJ Trans. Electr. Electron. Eng.* **2008**, *3*, 15–20. [CrossRef]
3. Ogasa, M. Onboard Storage in Japanese Electrified Lines. In Proceedings of the 14th International Power Electronics and Motion Control Conference, Ohrid, Macedonia, 6–8 September 2010. [CrossRef]

4. González-Gil, A.; Palacin, R.; Batty, P. Sustainable urban rail systems: Strategies and technologies for optimal management of regenerative braking energy. *Energy Convers. Manag.* **2013**, *75*, 374–388. [CrossRef]

5. Richardson, M.B. Flywheel Energy Storage System for Traction Applications. In Proceedings of the 2002 International Conference on Power Electronics, Machines and Drives, Bath, UK, 4–7 June 2002; pp. 275–279.

6. Liu, H.; Jiang, J. Flywheel energy storage—An upswing technology for energy sustainability. *Energy Build.* **2007**, *39*, 599–604. [CrossRef]

7. Thompson, R.C.; Kramer, J.; Hayes, R.J. Response of an urban bus flywheel battery to a rapid loss-of-vacuum event. *J. Adv. Mater.* **2005**, *37*, 42–50.

8. Gabash, A.; Li, P. Active-reactive optimal power flow in distribution networks with embedded generation and battery storage. *IEEE Trans. Power Syst.* **2012**, *27*, 2026–2035. [CrossRef]

9. Gabash, A.; Li, P. Flexible optimal operation of battery storage systems for energy supply networks. *IEEE Trans. Power Syst.* **2013**, *28*, 2788–2797. [CrossRef]

10. Iannuzzi, D. Improvement of the Energy Recovery of Traction Electrical Drives Using Supercapacitors. In Proceedings of the 13th IEEE Power Electronics and Motion Control Conference, Poznan, Poland, 1–3 September 2008; pp. 1469–1474.

11. Barrero, R.; Tackoen, X.; Van Mierlo, J. Improving Energy Efficiency in Public Transport: Stationary Supercapacitor Based Energy Storage Systems for a Metro Network. In Proceedings of the IEEE Vehicle Power and Propulsion Conference, Harbin, China, 3–5 September 2008; pp. 1–8.

12. Ciccarelli, F.; Iannuzzi, D.; Tricoli, P. Control of metro-trains equipped with onboard supercapacitors for energy saving and reduction of power peak demand. *Transp. Res. Part C Emerg. Technol.* **2012**, *24*, 36–49. [CrossRef]

13. Latkovskis, L.; Brazis, V.; Grigans, L. Simulation of on Board Supercapacitor Energy Storage System for Tatra T3A Type Tramcars. In *Modelling Simulation and Optimization*; InTech: Rijeka, Croatia, 2010.

14. Teymourfar, R.; Asaei, B.; Iman-Eini, H. Stationary super-capacitor energy storage system to save regenerative braking energy in a metro line. *Energy Convers. Manag.* **2012**, *56*, 206–214. [CrossRef]

15. Iannuzzi, D.; Tricoli, P. Metro Trains Equipped Onboard with Supercapacitors: A Control Technique for Energy Saving. In Proceedings of the 2010 International Symposium on Power Electronics, Electrical Drives, Automation and Motion (SPEEDAM), Pisa, Italy, 14–16 June 2010; pp. 750–756.

16. Iannuzzi, D.; Lauria, D.; Tricoli, P. Optimal design of stationary supercapacitors storage devices for light electrical transportation systems. *Optim. Eng.* **2012**, *13*, 689–704. [CrossRef]

17. Battistelli, L.; Fantauzzi, M.; Iannuzzi, D.; Lauria, D. Generalized Approach to Design Supercapacitor-Based Storage Devices Integrated into Urban Mass Transit Systems. In Proceedings of the IEEE 2011 International Conference on Clean Electrical Power (ICCEP), Ischia, Italy, 14–16 June 2011; pp. 530–534.

18. Teymourfar, R.; Farivar, G.; Iman-Eini, H.; Asaei, B. Optimal Stationary Super-Capacitor Energy Storage System in a Metro Line. In Proceedings of the 2011 2nd International Conference on Electric Power and Energy Conversion Systems (EPECS), Sharjah, The United Arab Emirates, 15–17 November 2011; pp. 1–5.

19. Grbović, P.J.; Delarue, P.; Le Moigne, P.; Bartholomeus, P. Modeling and control of the ultracapacitor-based regenerative controlled electric drives. *IEEE Trans. Ind. Electron.* **2011**, *58*, 3471–3484. [CrossRef]

20. Grbovic, P.J.; Delarue, P.; Le Moigne, P. Modeling and Control of Ultra-Capacitor Based Energy Storage and Power Conversion System. In Proceedings of the 2014 IEEE 15th Workshop on Control and Modeling for Power Electronics (COMPEL), Santander, Spain, 22–25 June 2014; pp. 1–9.

21. Ciccarelli, F.; Iannuzzi, D.; Lauria, D. Supercapacitors-Based Energy Storage for Urban Mass Transit Systems. In Proceedings of the 2011 14th European Conference on Power Electronics and Applications (EPE 2011), Birmingham, UK, 30 August–1 September 2011; pp. 1–10.

22. Zhang, Y.; Wu, L.; Hu, X.; Liang, H. Model and Control for Supercapacitor-Based Energy Storage System for Metro Vehicles. In Proceedings of the International Conference on Electrical Machines and Systems (ICEMS 2008), Wuhan, China, 17–20 October 2008; pp. 2695–2697.

23. Battistelli, L.; Ciccarelli, F.; Lauria, D.; Proto, D. Optimal Design of DC Electrified Railway Wayside Storage System. In Proceedings of the 2009 International Conference on Clean Electrical Power, Capri, Italy, 9–11 June 2009; pp. 739–745.

24. Barrero, R.; Tackoen, X.; van Mierlo, J. Stationary or onboard energy storage systems for energy consumption reduction in a metro network. *Proc. Inst. Mech. Eng. Part F J. Rail Rapid Transit* **2010**, *224*, 207–225. [CrossRef]

25. Vuchic, V.R. *Urban Transit Systems and Technology*; John Wiley & Sons: Hoboken, NJ, USA, 2007.

26. Wang, X.; Zang, H. Simulation study of DC traction power supply system for urban rail transportation. *Acta Simulata Syst. Sin.* **2002**, *12*, 1692–1697.

27. Han, L. A Study on the operation mode of medium voltage double-ring network and the relationship between interlock and inter-tripping in urban rail transit system. *Urban Rapin Rail Transit* **2004**, *1*, 018.

28. Yang, S.; Goto, K.; Imamura, Y.; Shoyama, M. Dynamic Characteristics Model of Bi-Directional DC-DC Converter Using State-Space Averaging Method. In Proceedings of the 2012 IEEE 34th International Telecommunications Energy Conference (INTELEC), Scottsdale, AZ, USA, 30 September–4 October 2012; pp. 1–5.